ACS OMEGA

http://pubs.acs.org/journal/acsodf

Article

Trimethine Cyanine Dyes as NA-Sensitive Probes for Visualization of Cell Compartments in Fluorescence Microscopy

Daria Aristova, Roman Selin, Hannah Sophie Heil, Viktoriia Kosach, Yuriy Slominsky, Sergiy Yarmoluk, Vasyl Pekhnyo, Vladyslava Kovalska, Ricardo Henriques, Andriy Mokhir, and Svitlana Chernii*

Cite This: *ACS Omega* 2022, 7, 47734–47746

Read Online

ACCESS | Metrics & More | Article Recommendations | Supporting Information

ABSTRACT: We propose symmetrical cationic trimethine cyanine dyes with β-substituents in the polymethine chain based on modified benzothiazole and benzoxazole heterocycles as probes for the detection and visualization of live and fixed cells by fluorescence microscopy. The spectral-luminescent properties of trimethine cyanines have been characterized for free dyes and in the presence of nucleic acids (NA) and globular proteins. The studied cyanines are low to moderate fluorescent when free, but in the presence of NA, they show an increase in emission intensity up to 111 times; the most pronounced emission increase was observed for the dyes **T-2** in the presence of dsDNA and **T-1** with RNA. Spectral methods showed the binding of all dyes to nucleic acids, and different interaction mechanisms have been proposed. The ability to visualize cell components of the studied dyes has been evaluated using different human cell lines (MCF-7, A2780, HeLa, and Hs27). We have shown that all dyes are cell-permeant staining nucleus components, probably RNA-rich nucleoli with background fluorescence in the cytoplasm, except for the dye **T-5**. The dye **T-5** selectively stains some structures in the cytoplasm of MCF-7 and A2780 cells associated with mitochondria or lysosomes. This effect has also been confirmed for the normal type of cell line—human foreskin fibroblasts (Hs27). The costaining of dye **T-5** with MitoTracker CMXRos Red demonstrates specificity to mitochondria at a concentration of 0.1 μM. Colocalization analysis has shown signals overlapping of dye **T-5** and MitoTracker CMXRos Red (Pearson's Coefficient value = 0.92 $\pm$ 0.04). The photostability study shows benzoxazole dyes to be up to ~7 times more photostable than benzothiazole ones. Moreover, studied benzoxazoles are less cytotoxic at working concentrations than benzothiazoles (67% of cell viability for **T-4**, **T-5** compared to 12% for **T-1**, and ~30% for **T-2**, **T-3** after 24 h). Therefore, the benzoxazole **T-4** dye is proposed for nucleic acid detection *in vitro* and intracellular fluorescence imaging of live and fixed cells. In contrast, the benzoxazole dye **T-5** is proposed as a good alternative to commercial dyes for mitochondria staining in the green-yellow region of the spectrum.

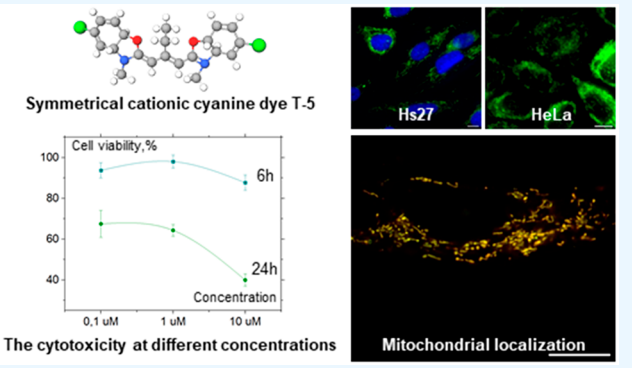

INTRODUCTION

Fluorescence microscopy has become a prevalent research method in modern cell biology since it gives incomparable opportunities to understand cellular processes. Fluorescent protein tags, organic dyes, carbon dotes, and other ways to fluorescently label biomolecules, compartments, and organelles provide a range of tools to investigate virtually any cellular process under the microscope.[1,2] For instance, it was reported that fluorescent carbon dots could stain nuclei in live and fixed cells. Besides, fluorescent carbon dots are widely applicable in imaging, sensing, drug delivery, and nucleolus-related biological behaviors.[3,4] Although carbon dots possess favorable spectral-luminescent characteristics, high photostability, and low cytotoxicity, they still suffer from low biomolecule selectivity and difficulties tuning biomolecule specificity. Most of them do not provide higher sensitivity and selectivity compared to other probes, mainly because of their low affinity and low enhancing/quenching efficiency induced by the analyte of interest.[5] Meanwhile, organic dyes are appealing stringing agents for live-cell visualization because of their simultaneously favorable optical properties, such as brightness and photostability, and high specificity toward biomolecules. In addition, they can be specifically designed to be membrane-permeable or membrane-impermeable, depending on what we want to observe—processes inside cells or on the surface.[6]

One of the most widespread classes of fluorescent organic dyes is cyanines. The history of cyanine dyes began more than

Received: August 15, 2022
Accepted: November 24, 2022
Published: December 13, 2022

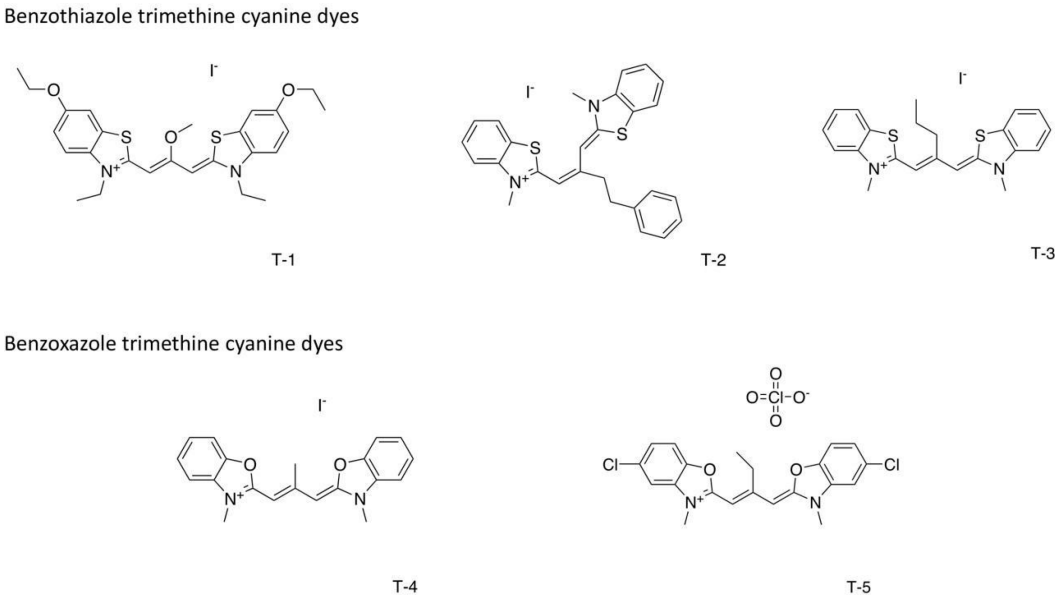

Figure 1. Chemical structure of studied symmetrical trimethine cyanine dyes **T-1**−**T-5**.

150 years ago when Williams reported the first synthesis of a blue solid in 1856.[7] Since then, cyanine dyes have been widely applied in many areas, especially fluorescent imaging, due to their good photophysical properties, high quantum yield values, excellent biocompatibility, and low toxicity to biological systems.[8,9] Monomethine and polymethine cyanine dyes are widely used for nucleic acid imaging. Their spectral properties are more advanced than those of other noncyanine dyes, such as Ethidium Bromide, DAPI, and Hoechst.[10] Moreover, they can be both membrane-permeant and membrane-impermeant. For example, TOTO or TO-PRO dyes for NA-staining in the gel or SYTOX dyes for dead-cell staining cannot penetrate inside a live cell. For instance, SYTOX Green nucleic acid stain quickly penetrates cells with compromised plasma membranes. This dye is a simple and quantitative dead-cell indicator successfully used to detect mammalian cells and bacteria viability.[11−13]

On the other hand, cell-permeant cyanine dyes, such as SYTO dyes, can be used for NA-staining in live cells. Nevertheless, these dyes do not have selectivity and can stain DNA and RNA; furthermore, they act as nuclear stains in live cells and can also stain other compartments, such as mitochondria.[14] For fluorescent probes, the low fluorescence quantum yield in the free state and the high quantum yield in the bound state, that is, a sharp increase in fluorescence intensity upon binding to a biomolecule, are essential.[15] These fluorescent dyes differ from fluorescent labels such as cyanines of the Cy3-Cy5 family dyes, which work as fluorescent labels attached chemically to the target molecule.[16] Dyes from the Cy family have high intrinsic fluorescence, quantum yield, and extinction coefficient and cannot be used as fluorescently sensitive probes for noncovalent binding and visualization of cell components. Thus, fluorescent probes should have a wide range of opposite properties, which is difficult to achieve in one molecule.[15]

Another example is SYBR family dyes, e.g., SYBR Green I, which intensely stained DNA in live cells but has the disadvantage that the fluorescence fades rapidly, and observation must be done as quickly as possible.[17] Moreover, it has been reported that monomethine cyanine dye Cyan 40 can be used for the two-photon fluorescent visualization of KB cells (oral epidermoid carcinoma).[18] We have also shown that this dye in low concentration could stain RNA-rich nucleoli without a background in the cytoplasm and have reported highly specific green-emitted monomethine cyanine dyes to stain RNA-containing structures in cells.[19] Besides this, our research group proposed near-infrared fluorescent probes among pentamethine cyanines and merocyanines as powerful far-red fluorescent probes applicable for the highly sensitive detection of albumins.[20,21]

Here we present our research of symmetrical cationic trimethine cyanine dyes with β-substituents in the polymethine chain based on substituted benzothiazole and benzoxazole heterocycles (ethyl group at the 3 positions and ethoxy group at the 6 positions for dye **T-1**, methyl group at the 3 positions for dyes **T-2**−**T-5** with additional chloro-group at the 5 positions for dye **T-5**) as probes for nucleic acids detection and visualization by fluorescence microscopy (Figure 1).

For the symmetrical β-methyl-substituted benzoxazole dye **T-4**, also known as Cyan 2-O, fluorescent sensitivity in complex with dsDNA was shown to be higher than the corresponding values for its benzothiazole analog Cyan 2.[22] It was also previously shown the fluorescent sensitivity to nucleic acids for trimethine cyanine dyes **T-2** (Cyan βPh) and **T-3** (Cyan βPr),[23] but their organelle specificity has not yet been investigated. For effective primary binding to DNA, cationic cyanine dyes are usually used.[24] It was previously shown that introducing substituents into β-position in the polymethine chain leads to a decrease in the fluorescence quantum yields of free dyes, with fluorescence response growing stronger with DNA presence as compared to carbocyanine dyes.[25]

Thus, the spectral-luminescent properties of trimethine cyanines have been studied in a free state in an aqueous buffer and in the presence of double-stranded DNA (dsDNA), RNA, human serum albumin (HSA), and beta-lactoglobulin (BLG). Furthermore, the ability of the studied dyes to penetrate the cell and stain its components has been investigated using human cancer MCF-7, A2780, HeLa, and normal Hs27 cell lines as models. First, different dye concentrations in live and fixed MCF-7 cells were used to determine the working conditions of each dye. Next, the ability to stain cells was confirmed for other cancer cell lines and normal Hs27 cells. According to

https://doi.org/10.1021/acsomega.2c05231
ACS Omega 2022, 7, 47734−47746

photostability evaluation, benzoxazole cyanine dyes (**T-4**, **T-5**) are more photostable than benzothiazoles (**T-1**, **T-2**, and **T-3**). We have tested dyes for cytotoxicity toward the A2780 cell line using standard MTT assay. Benzoxazoles are also shown lower cytotoxicity. Moreover, the dye **T-5** has a lower concentration selectivity toward cell components in the cytoplasm. Thus, the **T-5** dye was chosen for further studies. For this dye, a human foreskin fibroblast cell line (Hs27) was used to check whether the dye **T-5** at working concentration has the specificity staining pattern in cells. Finally, the mitochondria staining by benzoxazole **T-5** dye was confirmed by colocalization analysis with MitoTracker CMXRos Red.

MATERIAL AND METHODS

Materials. Dimethyl sulfoxide (DMSO), methanol (MeOH), distilled water, and 0.05 M Tris-HCl buffer (pH 7.9) were used as solvents. In addition, high molecular weight dsDNA (double-stranded DNA) from Salmon testis, RNA, human serum albumin (HSA), and beta-lactoglobulin (BLG) were purchased from Sigma-Aldrich Co. MitoTracker CMXRos Red, LysoTracker Deep Red, Hoechst 33342, and Thiazolyl Blue tetrazolium bromide (MTT) were purchased from ThermoFisher Scientific (Invitrogen).

The Synthesis of Symmetrical Trimethine Cyanine Dyes. *6-Ethoxy-2-((1Z,3Z)-3-(6-ethoxy-3-ethylbenzo[d]-thiazol-2(3H)-ylidene)-2-methoxyprop-1-en-1-yl)-3-ethylbenzo[d]thiazol-3-ium iodide (**T-1**).* Dye **T-1** was synthesized by condensation of 6-ethoxy-3-ethyl-2-methyl-1,3-benzothiazolium iodide with triethyl orthoformate.[26]

^{1}H NMR (400 MHz, dmso) δ 7.73 (d, J = 9.1 Hz, 2H), 7.69 (s, 2H), 7.20 (dd, J = 8.9, 2.6 Hz, 2H), 6.45 (s, 2H), 4.46 (q, J = 6.9, 6.9, 6.8 Hz, 4H), 4.10 (q, J = 7.0, 6.9, 6.9 Hz, 4H), 2.57 (s, 3H), 1.37 (m, 12H). ES-API MS (positive range) m/z: Calcd for $[C_{25}H_{28}N_2O_3S_2+H]^+$: 469.2. Found: 469.0

*3-Methyl-2-[3-(3-methyl-2,3-dihydro-1,3-benzothiazol-2-ylidene)-2-phenyl-1-propenyl]-trimethinium iodide (**T-2**).* Dye **T-2** also known as Cyan βPh[23] was synthesized as described[27,28] using iodomethylates of the corresponding salts of alkylthio derivatives of 3-methyl-benzothiazole.

*3-Methyl-2-[2-(3-methyl-2,3-dihydro-1,3-benzothiazol-2-ylidenemethyl)-1-pentenyl]-trimethinium iodide (**T-3**).* Dye **T-3** also known as Cyan βPr[23] was synthesized as described[27,28] using iodomethylates of the corresponding salts of alkylthio derivatives of 3-methyl-benzothiazole.

*3-Methyl-2-[2-methyl-3-(3-methyl-2,3-dihydro-1,3-benzooxazol-2-ylidene)-1-propenyl)-1,3-benzooxazol]-trimethine iodide (**T-4**).* B-methyl-substituted benzoxazole dye **T-4** also known as Cyan 2-O(J6)[22,29] was synthesized as described in refs 22 and 23 using the orthoester method.

*5-Chloro-2-((E)-2-((Z)-(5-chloro-3-methylbenzo[d]thiazol-2(3H)-ylidene)methyl)but-1-en-1-yl)-3-methylbenzo[d]-thiazol-3-ium perchlorate (**T-5**).* Dye **T-5** was synthesized by condensation of 5-cloro-2,3-dimethylbezoxazole ethyl sulfate with triethyl orthoformate by the procedure described in ref 30.

^{1}H NMR (400 MHz, dmso) δ 7.91 (m, 2H), 7.83 (m, 2H), 7.43 (d, J = 8.9 Hz, 2H), 5.83 (m, 2H), 3.74 (s, 6H), 2.50 (m, 2H +DMSO), 1.31 (t, J = 7.4, 7.4 Hz, 3H). ES-API MS (positive range) m/z: Calcd for $[M + H]^+$: 434.0. Found: 434.0.

The structure of the compounds was confirmed by NMR H^1 spectroscopy and element analysis.

The Preparation of Stock/Working Solutions of Dyes, Nucleic Acids, and Proteins. Dye stock solutions were prepared by dissolving the dyes at 2 mM concentration in DMSO. Working solutions of free dyes were prepared by diluting the dye stock solution in 0.05 M Tris-HCl buffer or MeOH. The dye working concentrations amounted to 5 μM. Working solutions of the dyes in the presence of nucleic acids were prepared by adding the aliquot of the dye stock solution to the nucleic acid working solution. Nucleic acid stock solutions were equal to 6×10^{-3} M for dsDNA from Salmon testis and 1.2×10^{-2} M for RNA. Working solutions were prepared by diluting the stock solution 100 times to final dsDNA and RNA concentrations of 6×10^{-5} M bp and 1.2×10^{-4} M bases, respectively. Protein stock solutions (HSA, BLG) were prepared by dissolving in 0.05 M Tris-HCl buffer pH 7.9 at a concentration equal to 0.2 mg/mL. Working solutions were prepared by adding the dye aliquots to the protein stock solutions. All working solutions were prepared immediately before the experiments.

Spectroscopic Measurements. Spectroscopic measurements were performed in a standard quartz cuvette (10 × 10 mm). Fluorescence excitation and emission spectra were recorded using the Cary Eclipse fluorescence spectrophotometer (Varian, Australia). Absorption spectra were registered using the spectrophotometer Shimadzu UV-3600. All the spectral-luminescent characteristics of dyes were studied at room temperature.

Cell Culture Cultivation. The human breast adenocarcinoma cell line (MCF-7) was obtained from the Bank of Cell Lines of the R. E. Kavetsky Institute of Experimental Pathology, Oncology and Radiobiology, NASU (Ukraine). Human foreskin fibroblasts HFF Hs27 (ATCC CRL-1634) were gifted by Jonathan Howard from the Instituto Gulbenkian de Ciência (Portugal). The human ovarian cell line (A2780) was purchased from Sigma-Aldrich. HeLa(CCL-2) cell line was obtained from ATCC.

The MCF-7 and HHF Hs27 cells were cultivated in DMEM culture medium (Gibco, USA) supplemented with 10% fetal bovine serum (FBS), 4 mM L-glutamine, 50 units/mL penicillin, and 50 μg/mL streptomycin at 37 °C in 5% CO_2. In addition, A2780 cells were cultivated in RPMI-1640 medium supplemented with 10% FBS, 1% L-glutamine, and 1% penicillin/streptomycin at 37 °C in 5% CO_2 to 80−90% confluence. Cells were detached from the flask by using trypsin/EDTA solution (0.025%/0.01%, w/v, Biochrom GmbH, Germany) in DPBS.

MCF-7 cells were seeded on sterile glass coverslips in 24-well plates 48 h before further experiments at the concentration of 2×10^4 cells per well in 1 mL of DMEM medium containing 10% FBS, 4 mM glutamine, 50 units/mL penicillin, and 50 μg/mL streptomycin. HeLa and Hs27 cells were seeded in an 8-well-chambered cover glass with #1.5 high-performance cover glass (Cellvis) 24 h before the experiment at the concentration of 2×10^4 cells per well in 0.4 mL of DMEM medium containing 10% FBS, 4 mM glutamine, 50 units/mL penicillin, and 50 μg/mL streptomycin. The samples were stored at 37 °C in 5% CO_2 overnight. The A2780 cells were seeded at 80 cells/μL per glass-bottom fluorescent dish (μ-Dish 35 mm, high, ibidi GmbH, Germany) in RPMI-1640 medium with 5% FBS. Cell number counting was performed using a hemocytometer or via Guava easyCyteTM 6−2L Flow cytometer (Merck Millipore, Darmstadt, Germany).

MCF-7 Live-Cell and Fixed Cell Fluorescence Microscopy. For live-cell imaging of MCF-7, cells were washed twice with preheated PBS. After that, the cells were incubated with cyanine dyes in FluoroBrite DMEM (Gibco, USA) without FBS for 30 min at 37 °C in 5% CO_2. Cells were then rewashed with

https://doi.org/10.1021/acsomega.2c05231
ACS Omega 2022, 7, 47734−47746

Table 1. Characteristics of Vis Absorption Spectra of Dyes[a]

	Tris-HCl buffer, pH 7.9	Tris-HCl buffer, with RNA	Tris-HCl buffer, with dsDNA	MeOH	
dye	λ_{max} (nm)	λ_{max} (nm)	λ_{max} (nm)	λ_{max} (nm)	ε (10^5 $M^{-1}cm^{-1}$)
T-1	500/552*	502*/562	461*/530*/565	559	1.1
T-2	507*/543	514*/548	510*/544	545	0.7
T-3	504*/541	514*/545	512*/544	543	1.2
T-4	460*/486	463*/487	470*/495	460*/488	0.9
T-5	465*/492	475*/497	473*/497	467*/494	1.7

[a] λ_{max}, maximum wavelength of the absorption spectrum; *, characteristic shoulder at the edge of the main band; ε, molar extinction coefficient at λ_{max}, calculated from the main absorption maximum optical density.

PBS and placed in FluoroBrite DMEM. For fixed-cell imaging, MCF-7 cells were fixed in 10% neutral buffered formalin (Sigma-Aldrich, USA) for 15 min at room temperature (RT). Next, cell membranes were permeabilized with 0.2% Triton X-100 in PBS for 10 min at RT. After that, cells were incubated with 10 mM cupric sulfate and 50 mM ammonium acetate (pH 5.0) for 30 min at RT to reduce autofluorescence. Next, cyanine dyes in PBS were added to the samples for 30 min at RT in the dark. During incubations, cells were washed three times with PBS. In the end, samples were embedded into Mowiol 4−88 mounting medium (Sigma-Aldrich, USA) containing 2.5% DABCO (Sigma-Aldrich, USA). Microscopy image acquisition of MCF-7 cells was performed using Leica DM 1000 epifluorescent microscope with the following excitation (ex) filters: ex 355−425 nm for Hoechst 33342, ex 450−490 nm for benzoxazole dyes, and ex 515−560 nm for benzothiazoles.

A2780, HeLa, and Hs27 Live-Cell Fluorescence Microscopy and Colocalization Study. HeLa and HHF Hs27 cells were washed twice with preheated PBS for live-cell imaging. After that, a solution of Hoechst 33342 in DMEM culture medium (Gibco, USA) was added, and cells were left for 10 min at 37 °C in 5% CO_2. The cells were then rewashed twice with PBS, and the solution of the cyanine dyes was added to the DMEM culture medium. Cells were incubated for 20 min at 37 °C in 5% CO_2 and rewashed twice after with PBS. FluoroBrite DMEM medium was then added. Images were acquired with the commercial Nikon High Content Screening microscope equipped with an Andor Zyla 4.2 sCMOS camera and heating and atmospheric control chamber, using a 40× 1.30NA Oil objective and excitation lasers: 380 nm for Hoechst 33342, 480 nm for benzoxazole dyes **T-4**−**T-5**, 550 nm for benzothiazole dyes **T-1**−**T-3**. Images were proceeded using free software Fiji/ImageJ v1.53f51.[31]

For the **T-5** colocalization with LysoTracker DeepRed, the A2780 cell line was used. Every fluorescent dish with 2 mL of total volume was left at 37 °C in 5% CO_2 overnight. On the next day, for the colocalization study, solutions of Hoechst 33342, LysoTracker DeepRed, and the dye **T-5** in DMSO were added into separate and the same dishes for 30 min of incubation for **T-5**, 15 min for Hoechst 33342 and LysoTracker DeepRed (1 and 0.1 μM for **T-5**, and 50 nM for LysoTracker DeepRed). For other dyes, the following concentrations were used: 10 μM for **T-1**, 1 μM for **T-2** and **T-3**, and 0.1 μM for **T-4**. Then the cells were washed twice with DPBS, and 5% Medium (2 mL) was added. The fluorescence images were taken with a Zeiss Axio Vert.A1 and filter set: ex 625−655/em 665−715 nm (deep red) for the detection of LysoTracker DeepRed, ex 335−383/em 420−470 nm (blue) for the detection of Hoechst 33342, and ex 450−490/em 500−550 nm (green) for the detection of **T-5**, **T-4**, and ex 538−562/em 570−640 nm for dyes **T-1**, **T-2**, and **T-3**. Objective: 40×1.30. Oil (DIC). Images were proceeded using free software Fiji/ImageJ v1.53f51.[31]

For the colocalization study with MitoTracker CMXRos Red, the HHF Hs27 cell line was used. Before the experiment, the growth medium was removed, and the Hs27 cells were washed twice with preheated PBS. After that, the cells were incubated with MitoTracker CMXRos Red in DMEM culture medium (Gibco, USA) for 15 min at 37 °C in 5% CO_2. The cells were then rewashed with PBS, and the solution of the cyanine dye **T-5** was added to FluoroBrite DMEM medium. Cells were incubated with this solution for 20 min at 37 °C in 5% CO_2. Images of Hs27 cells were acquired on the Zeiss LSM980 system, equipped with a dark heating and atmospheric control chamber, using Airyscan SR mode, a 63× 1.4NA Oil immersion objective, with 488 nm laser for the excitation of the dye **T-5** and 561 nm laser for the excitation of MitoTracker CMXRos Red with the same laser power and scanning speed for all acquisitions. Images were acquired at 37 °C in 5% CO_2. Obtained Airyscan images were processed with ZEN Blue 3.3 and analyzed using free software Fiji/ImageJ v1.53f51.[31] For colocalization analysis, seven images of cells stained with **T-5** dye and MitoTracker CMXRos Red were acquired, and Pearson's coefficient of correlation was obtained using Fiji plugin JACoP[32] with a followed average value and standard deviation calculation.

The Time-Dependent Photostability Study. The irreversible bleaching of trimethine dyes fluorescence was monitored under constant irradiation as a function of time. HeLa and HHF Hs27 cells were seeded at concentration 2×10^4 cells per well in 8 Well Chambered Cover Glass with #1.5 high-performance cover glass (Cellvis) 24 h prior to the experiment. Before the experiment, the growth medium was removed, and the cells were washed twice with preheated PBS. After that, the cells were incubated with Hoechst 33342 in DMEM culture medium (Gibco, USA) for 10 min at 37 °C in 5% CO_2. Then cells were rewashed with PBS, and a solution of the cyanine dyes in DMEM culture medium was added at their working concentrations (given in Figure 6) for 20 min. After cells were rewashed twice with PBS and FluoroBrite DMEM was added. Fluorescence was excited with 380 nm laser for Hoechst33342, 550 nm for **T-1**−**T-3**, and 480 nm for **T-4**−**T-5** using the commercial Nikon High Content Screening microscope equipped with an Andor Zyla 4.2 sCMOS camera and heating and atmospheric control chamber, using a 40× 1.30NA Oil objective. The fluorescence intensity was measured using a special mode in NIS-Elements AR 4.60 software for 8 min. The software recorded values every 0.05 or 0.1 s. Fluorescence intensity was normalized as I/I_0, where I_0 is the fluorescence intensity at zero time point (0 min 00 s) and I is the fluorescence intensity at a given time point (up to 8 min).

Cytotoxicity Assay. Cytocompatibility of trimethine dyes toward A2780 cells was assessed by the standard MTT

https://doi.org/10.1021/acsomega.2c05231
ACS Omega 2022, 7, 47734−47746

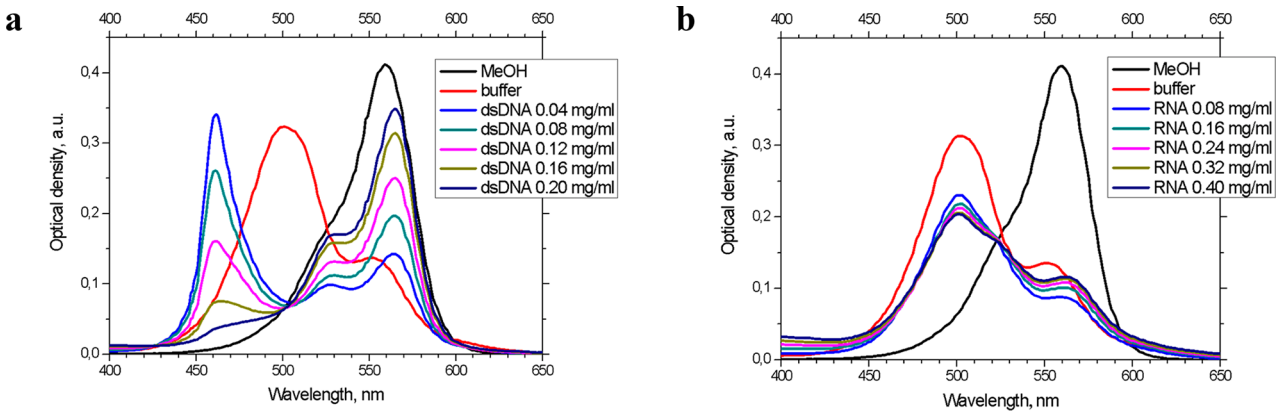

Figure 2. Absorption spectra of the trimethine cyanine dye **T-1** in dsDNA (a) and RNA (b) presence in 0.05 M Tris-HCl (pH 7.9). Dye concentration 5 μM.

cytotoxicity assay based on the reduction of MTT tetrazolium to MTT formazan pigment by the metabolic activity of living cells. For this, A2780 cells were seeded at the concentration of 250 cells/μL per well in a 96-well plate. Three separate plates with three replicate wells were used for each DMSO-containing control and tested concentrations. **T-1**−**T-5** dyes in three different concentrations of 10, 1, and 0.1 μM (1 μL of DMSO stock solution) were added to the cells (100 μL per well into 96-well plates) and incubated for 6 and 24 h. After incubation, the MTT dye (20 μL in PBS, 5 mg/mL stock solution) was added to the cells and incubated for 3 h. Then, 10% SDS solution (90 μL per well) was added. After overnight incubation, the absorption of suspensions at λ 590 and 690 nm was measured. The value of A(590 nm)−A(690 nm) counted as a value proportional to the percentage of living cells (compared to DMSO-containing samples as control ones).

RESULTS AND DISCUSSION

Photophysical Properties of the Symmetrical Trimethine Cyanine Dyes. We have obtained Vis spectra of the trimethine cyanine dyes in methanol and aqueous buffer 0.05 M Tris-HCl, pH 7.9 (Table 1, Figure S1). The absorption maxima of the trimethine cyanines in methanol are located in the range of 488−559 nm, and the molar extinction values are in the range (0.7−1.7) × 10^5 M^{-1} cm^{-1}. The spectra of the cyanine dyes in methanol are suggested to belong to their monomeric form. We have observed that the positions of the absorption maximum are different and depend on heterocycles in dyes structures. Thus, the maximums of benzothiazole cyanines (**T-1**, **T-2**, **T-3**) are located in the longer wavelength region of the spectrum (543−559 nm) compared to the benzoxazole dyes **T-4** and **T-5** (488−494 nm). The absorption of cyanines is determined by the existence of the delocalized π-electron system. Therefore, it depends on the length of the polymethine chain. At the same time, heavy atoms in the heterocycle change the effective length of the π-electron system, affecting the absorption and emission maxima.[33] As most symmetric cyanines, **T-1**, **T-4**, and **T-5** have an utter short-wavelength vibronic maximum as a characteristic shoulder at the short-wavelength edge of the main band in their absorption spectra (Figure S1a).[34]

The aggregation morphology of dyes can significantly affect their optical properties.[35] Benzoxazole dyes (**T-4**, **T-5**) are presented in monomeric form in methanol and aqueous buffer solution (Figure S1a, b). Benzothiazole cyanines **T-2** and **T-3** undergo self-organization in an aqueous solution. The reduction in the absorption of the monomer band and the appearance of a new maximum at shorter wavelengths 504−507 nm has been observed (Figure S1a, b). In the case of the **T-3**, the ε of the aggregates maximum is almost equal to the ε of the monomers maximum. The addition of these hypsochromic peaks is a hallmark of forming H-aggregates (H-type dimers).[33,36] Dimerization of cyanines can lead to longer excited singlet lifetimes but weak or no fluorescence.[35] The dye **T-1** in the buffer solution exists as H-dimers with a blue-shifted absorption peak at 502 nm compared to the monomers (552 nm) with higher ε (Figure S1b). We can suggest the strong aggregation behavior of benzothiazole dyes (**T-1**, **T-2**, **T-3**) in an aqueous solution.

We have also estimated absorption spectra in the presence of dsDNA and RNA (Table 1, Figure S1c, d). A characteristic feature of the cyanine spectra in the presence of dsDNA and RNA is the bathochromic shift of the monomer absorption maxima relative to free dyes up to 10 nm (Table 1). According to the literature, such behavior is suggested to be caused by a different immediate environment of chromophores due to complexation with nucleic acids.[37] The long-wavelength shift in the absorption maxima is known to be observed due to a decrease in the nucleophilicity of the environment.[37]

In addition, there is an increase in optical density for monomer bands and a decrease for H-type dimer bands in the case of **T-2** and **T-3** dyes (Figure S1c, d). This behavior indicates a dye-nucleic acid interaction, preferably in monomeric form. For **T-4** and **T-5** dyes, the shoulder at the edge of the main band disappears almost entirely in the presence of dsDNA (Figure S1c) with an immediate effect in the presence of RNA (Figure S1d). This behavior also indicates the dye-nucleic acid interaction in monomeric form.

For the dye **T-1**, different aggregation behavior is observed depending on the type of nucleic acid (Figure 2a, b). Thus, in the presence of RNA, broad maxima of the monomer (longwave) and dimer (shortwave) are observed (Figure 2b). The optical density of the dye monomer is twice less than the optical density of the dimer. However, the shape of the spectra differs slightly from that of the free dye in the buffer solution. Increasing RNA concentration leads to a slightly decreasing absorbance of the H-band, indicating the slow breakdown of the H-aggregates with the minimal recovery of the monomer bands, which reach equilibrium at the concentration of 0.32 mg/mL. Further addition of RNA does not affect the H-dimers of the dye **T-1**.

https://doi.org/10.1021/acsomega.2c05231
ACS Omega 2022, 7, 47734−47746

Table 2. Spectral-Luminescent Properties of Trimethine Cyanine Dyes in a Free State and the Presence of Nucleic Acids in 0.05 M Tris-HCl Buffer (pH 7.9)[a]

	free state				with RNA				with dsDNA			
	$\lambda_{ex.}$ (nm)	$\lambda_{em.}$ (nm)	I (a.u.)	ΔS (nm)	$\lambda_{ex.}$ (nm)	$\lambda_{em.}$ (nm)	I^{RNA}/I (t)	ΔS^{RNA} (nm)	$\lambda_{ex.}$ (nm)	$\lambda_{em.}$ (nm)	I^{DNA}/I (t)	ΔS^{DNA} (nm)
T-1	562	580	15	18	567	584	75	17	566	578	111	12
T-2	554	567	46	13	550	575	83	25	545	569	56	24
T-3	552	564	118	12	548	574	33	26	545	567	15	22
T-4	488	501	124	12	499	511	65	12	500	511	73	11
T-5	493	506	312	13	505	519	26	14	505	517	37	12

[a] $\lambda_{ex.}$ ($\lambda_{em.}$), maximum wavelength of fluorescence excitation (emission) spectrum; I, emission intensity of dye in a free state (I) and in the presence of nucleic acids (I^{RNA}, I^{DNA}); a.u., arbitrary units; t, the number of times; ΔS, Stokes shift.

In the presence of dsDNA, besides the absorption maxima of the monomer and dimer of the **T-1**, there is also the third blue-shifted absorption maximum band that appears at lower wavelengths with a large Stokes shift relative to the monomer (104 nm, Figure 2a). In most cases, the H-type aggregates of cyanine dyes are limited to H-dimers and extended H-type aggregates when dye molecules form head-to-head H-type aggregates, and ideally appear commonly as a broad absorption band with quenching properties.[38] As an exception, the formation of the chiral arrangement of cyanine dyes with a narrow absorption band, a huge Stokes shift of cyanine dye bound to gemini surfactants, has been previously shown.[35] We can assume a similar aggregation behavior of the **T-1** dye on the dsDNA template (Figure 2a). This effect is not observed for RNA, most likely because it exists mainly in a single-stranded form. Thus, increasing the concentration of dsDNA leads to a gradually decreasing absorbance of the narrow absorption H-band, indicating the progressive disruption of the H-aggregates. As shown in Figure 2a, the second H-band almost completely disappears upon adding 0.2 mg/mL of dsDNA. Based on the absorption spectra, all the dyes studied interact with nucleic acids but have different preferable types of binding.

Spectral-luminescent properties of the symmetrical trimethine cyanine dyes free in Tris-HCl buffer pH 7.9 solution and the presence of nucleic acids are presented in Table 2. These dyes possess low to moderate fluorescence intensity in the aqueous buffer. Introducing bulky substituents into the cyanine polymethine chain could decrease its free-state fluorescence intensity compared to the unsubstituted analogs. This effect is observed for the dye **T-2** compared to **T-3**, which are structurally identical except for the substituent in the polymethine chain. Similar to the main absorption bands, fluorescence emission maxima depend on the presence of heavy atoms in heterocycles. In the case of the benzoxazole ring, trimethine cyanine fluorescence is observed at 501−506 nm, while those of benzothiazole have a maximum of 564−580 nm. The Stokes shift value for free dyes is in the range of 12 to 18 nm.

The addition of nucleic acids leads to an increase in fluorescence intensity (15−111 times). The maximums of the fluorescence emission spectra of dyes in the presence of RNA and dsDNA are shifted in the long-wavelength region for 4−13 nm. The increase in Stokes shift is observed for **T-2** and **T-3** dyes in the presence of nucleic acids (Table 2). The most pronounced fluorescent response is observed for **T-1** in the presence of dsDNA (111 times) and up to 83 times for dye **T-2** in the presence of RNA. The fluorescent sensitivity of the studied dyes to dsDNA and RNA is not similar, as seen in Table 2. The **T-2** and **T-3** dyes were 1.5−2.2 times more sensitive to RNA than to dsDNA. **T-1** dye was 1.5 times more sensitive to dsDNA than to RNA. For other dyes, the I^{RNA}/I^{DNA} ratio was 0.7−0.89 (Table 2), probably meaning no selective specificity to NA.

The binding of dyes to nucleic acids, depending on their structure, can occur by (i) electrostatic interaction between the cationic dyes and the anionic phosphodiester groups of the dsDNA/RNA backbone, (ii) intercalation between adjacent base pairs, (iii) minor groove binding,[10,39] and (iv) half-intercalation interaction mode.[40,41] It is also known that groove binding to DNA becomes more prevalent for the cyanine dyes with more than one methine bridge. For example, trimethine-bridged cyanine dyes have been shown to bind to the minor DNA groove as monomers and dimers.[42]

For dyes **T-2** and **T-3** with nucleic acids (both dsDNA and RNA), there is an increase in the value of the Stokes shift (ΔS) by 11−16 nm. The increase in the ΔS for cyanine dyes occurs with increasing electron asymmetry of the molecule.[43] The electrical asymmetry of the dye molecule increases with the half-intercalating mode of binding to DNA when the molecule is simultaneously oriented in the dipole medium between base pairs and negative charges of phosphate groups in the groove. Thus, given the increase in ΔS values and the partial destruction of dimers in the absorption spectra in the presence of dsDNA, it can be assumed that the dyes **T-2** and **T-3** also bind to dsDNA due to a half-intercalating mechanism in monomeric form.

As mentioned above, we have observed that dyes **T-2** and **T-3** have slightly higher fluorescence sensitivity to RNA than dsDNA. The different sensitivity of benzothiazole cyanine dyes for different NA was explained in.[44] These dyes could selectively form fluorescent J-aggregates when bound to the DNA molecule. However, based on our results in Table 1, the studied benzothiazole cyanine dyes do not form J-aggregate peaks in the absorbance spectra. Thus, we have considered another explanation for this phenomenon. For example, forms of secondary structures of RNA make the binding sites for these dyes more preferable. In ref 45, perturbations of the A-form helix of the RNA molecule induced by un- or mispaired bases widen the major groove to provide a surface-exposed binding pocket, and pockets found in RNA present varying degrees of electronegative potentials. The various folds adopted by the different secondary structures offer specific binding sites further characterized by their electronegative landscape. Binding to such pockets can lead to changes in the electrical asymmetry of the dye molecules, which is confirmed by an increase in the ΔS for **T-2** and **T-3** in the presence of RNA. Therefore, we can suggest that the addition of the longer β-substituents in the polymethine chain led to stronger binding to the secondary structure of the RNA molecule than dsDNA.

The most significant changes occur in the electronic spectra of the dsDNA complex with the **T-1** dye (Figure 2a), which shows the highest increase in fluorescence in its presence. Redis-

https://doi.org/10.1021/acsomega.2c05231
ACS Omega 2022, 7, 47734−47746

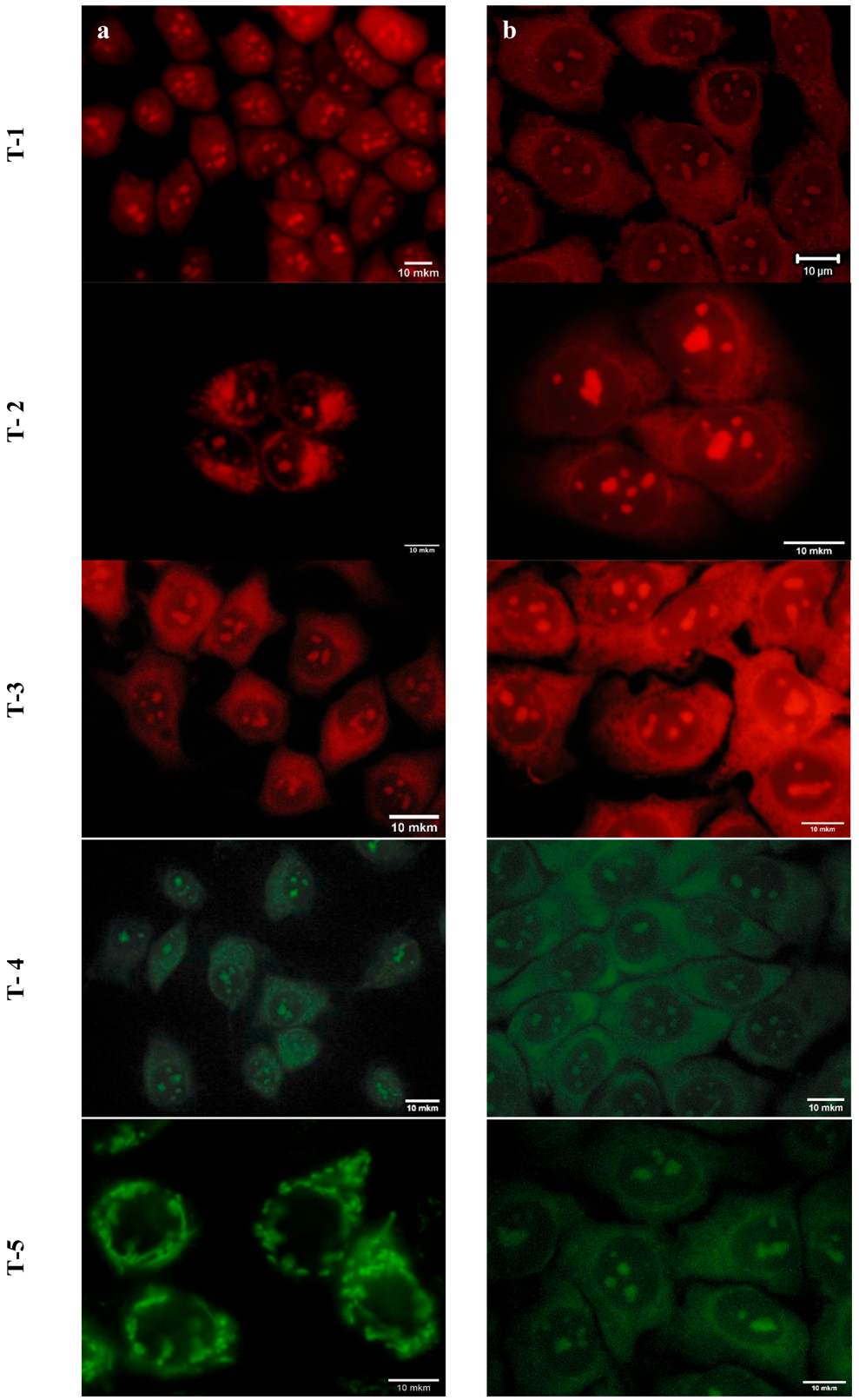

Figure 3. Fluorescence imaging of live (a) and fixed (b) MCF-7 cells stained with the studied dyes **T-1**−**T-5** (dyes concentrations for live cell imaging: **T-1**−10 μM; **T-2**, **T-3**−1 μM; **T-4**, **T-5**−0.1 μM; for fixed cell imaging: **T-1**, **T-4**−1 μM; **T-2**, **T-3**, **T-5**−0.1 μM). Scale bars: 10 μm.

tribution between three electronic bands upon adding dsDNA indicates three distinct binding modes. We suggest that the addition of dsDNA leads to the formation of the arrangement of dye molecules at 461 nm using dsDNA as a template. These aggregates can interact with dsDNA through electrostatic binding or small groove binding. Subsequent addition of dsDNA leads to the destruction of the aggregates and increases the absorption maximum of the monomers, accompanied by an

https://doi.org/10.1021/acsomega.2c05231
ACS Omega 2022, 7, 47734−47746

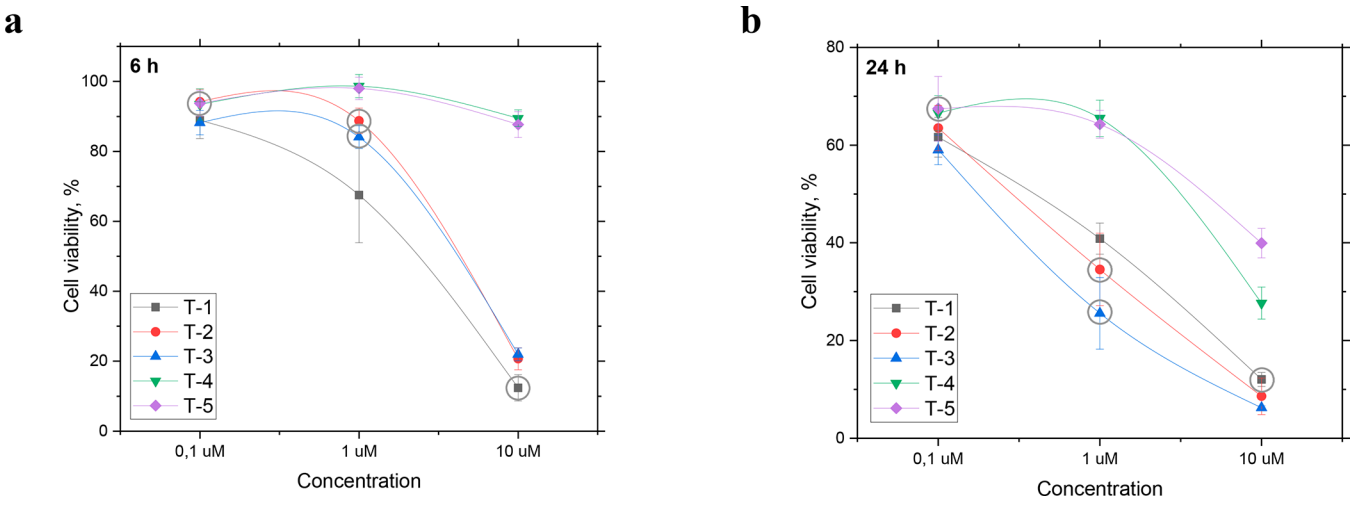

Figure 4. Comparisons of the cytotoxicity of trimethine cyanines **T-1**−**T-5** at different concentrations (0.1, 1, and 10 μM) toward A2780 cells for 6 (a) and 24 (b) h. Working concentrations are marked with a circle. The standard deviation is presented as error bars.

increase in fluorescence. The other absorption peak at 565 nm proportionally increases with the destruction of aggregates and is most probably associated with an intercalated complex. These observations indicate that the dye **T-1** is bound to dsDNA in monomeric form with an increased DNA/dye ratio and that the preferred binding mode can be intercalative. In the presence of proteins (HSA and BLG), no significant increase in the fluorescence intensity of the dyes was observed (Table S1). Thus, the fluorescence specificity and interaction with nucleic acids by spectral methods are shown for all studied dyes.

The Fluorescence Microscopy Study of Staining Properties of Trimethine Cyanine Dyes in Cancer Cells. To understand if the studied trimethine cyanine dyes are suitable for cell visualization by fluorescence microscopy, we have stained human breast cancer cells MCF-7 with the following visualization. We suggested that the dyes may be specific for nucleic acids in cells (RNA-containing cell organelles or nuclei). Therefore, we have investigated the ability of dyes to penetrate the cell and stain its components (Figure 3).

The MCF-7 cell line was chosen for this purpose because it is a well-characterized, widely used breast cancer model with adherent and nicely spread cells suitable for imaging subcellular architecture.[46] MCF-7 cells were incubated with different dye concentrations (10 μM, 1 μM, 0.1 μM) to determine the working conditions of the dyes. We have used 450−490 nm irradiation for benzoxazoles and 515−560 nm irradiation for benzothiazoles to excite the fluorescence of the cyanine dyes studied.

We have found that all dyes proved to be membrane-permeant and stain the subcellular components both in live and fixed cells with different sensitivity (Figure 3). Optimal results for live cell staining were obtained at the following concentrations: 10 μM for dye **T-1**, 1 μM for dyes **T-2** and **T-3**, and 0.1 μM for dyes **T-4** and **T-5**. For fixed cell staining, optimal conditions were 1 μM for dyes **T-1**, and **T-4**, 0.1 μM for dyes **T-2**, **T-3**, and **T-5**. All studied dyes penetrated the nuclear membrane and stained large structures within the nucleus, most probably nucleoli, except for the dye **T-5**, which at the concentration of 0.1 μM, specifically stains some structures in the cytoplasm of MCF-7 cells.

In fixed cells, the dyes studied possessed a similar behavior with slightly stronger fluorescence in the cytoplasm. The exception is the **T-5** dye, which shows a different staining pattern from live to fixed cells at the same concentration of 0.1 μM: (i) staining compartments (mitochondria or lysosomes) in the cytoplasm without nucleus penetration in live cells and (ii) penetrates the nucleus and staining nucleoli with background fluorescence in the cytoplasm in fixed cells. Usually, a charge of the mitochondria membrane is involved in binding dyes to this organelle, but in fixed cells, the charge disappears, and binding does not occur. Thus, we don't see the dye accumulation in the cytoplasm and, consequently, weak fluorescent green background with quite a bright staining of nucleoli.

Staining two more cancer cell lines (human ovarian adenocarcinoma cell line A2780 and cervical cancer cell line HeLa) was performed to check if the staining pattern remains the same regardless of cell type. It was shown that dyes penetrate cytoplasm membranes and stain A2780 and HeLa cell compartments at the same working concentration as MCF-7 (Figures S2 and S3).

The cytocompatibility of the dyes has been investigated using cell line A2780. A standard cytotoxicity MTT test was performed for 6 and 24 h (Figure 4). After 24 h, studied benzoxazoles are less cytotoxic to cancer cells at working concentrations than benzothiazoles (67% of cell viability compared to 12% for **T-1** and ∼30% for **T-2**, **T-3**). In contrast, after 6 h, benzoxazoles **T-4**/**T-5** and benzothiazoles **T-2**/**T-3** at working concentrations show almost the same cytotoxicity (∼85% of cell viability). However, the toxicity of benzothiazoles, but not benzoxazoles, increases with increasing concentration.

Thus, the dyes **T-4** and **T-5** have the highest cytocompatibility, ensuring the applicability of this dye as a potentially useful probe for long-term live-cell imaging.

Staining of Human Foreskin Fibroblasts by Trimethine Cyanine Dyes. The membrane potential (V_m) in cancer cells changes. Namely, electrophysiological analyses in many cancer cell types have shown a depolarized V_m.[47] As a result, the cancer cell surface is negatively charged, and the cytoplasm has a positive charge. Furthermore, cancer cells have a higher intracellular pH (≥7.4) and a lower extracellular pH (∼6.7−7.1).[48] These pH conditions in cancer cells are entirely opposite to the pH gradient of normal cells.[49,50] This hallmark of cancer cells lies in the overactivation of plasma membrane ion pumps and transporters that extrude protons and intrude other ions.

https://doi.org/10.1021/acsomega.2c05231
ACS Omega 2022, 7, 47734−47746

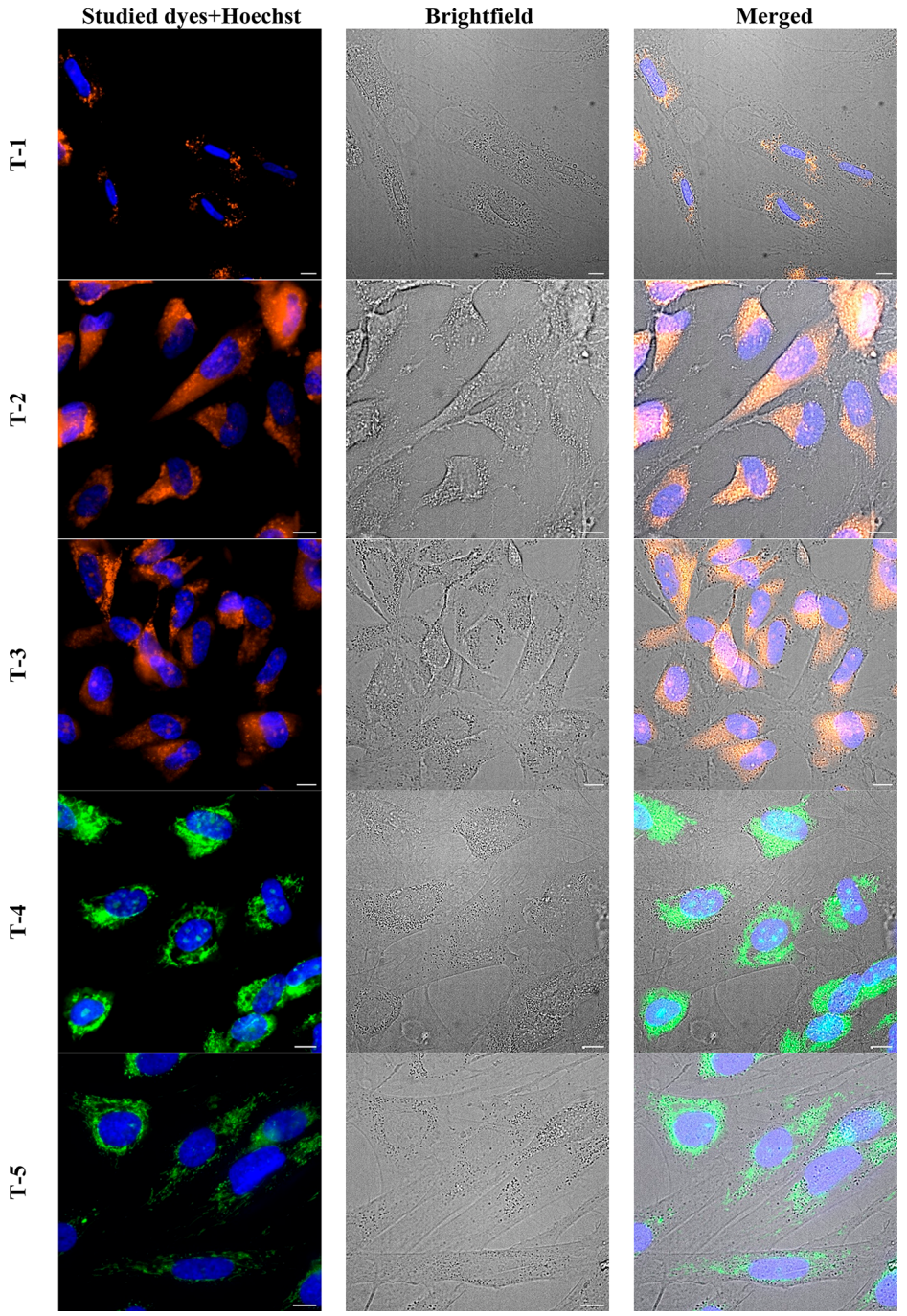

Figure 5. Fluorescence imaging of live Hs27 cells stained with the studied dyes **T-1**−**T-5**. (**T-1** at the concentration of 10 μM, **T-2**, and **T-3** dyes at the concentration of 1 μM, **T-4**, and **T-5** at the concentration of 0.1 μM). Scale bars: 10 μm.

Moreover, the mitochondria membrane of cancer cells is hyperpolarized compared to normal cells.[51] Another characteristic of cancer cell metabolism is the higher ROS levels observed in the tumor cells than in healthy ones. Because the studied dyes carry a positive (cationic) charge, it was decided to test whether differences in these parameters in cancer and normal cells affect the ability of the dyes to penetrate the cell and their organelle specificity. For this purpose, the human foreskin fibroblast cell line (Hs27) was selected as a model object for live-cell imaging.

The fluorescent microscopy study has shown that all studied dyes keep the same staining pattern in normal Hs27 cells as in cancer cells MCF-7, except for dye **T-1**. Thus, this dye does not penetrate the nucleus of Hs27 and stains some roundish structures in the cytoplasm that could be swollen mitochondria or lysosomes (Figure 5).

The Time-Dependent Photostability of Trimethine Cyanine Dyes in HeLa and Hs27 Cells. Photodegradation, commonly referred to as photobleaching, depletes the fluorophore concentration under prolonged irradiation and represents one of the most severe limitations in fluorescence microscopy.[33] We have investigated the photostability of dyes under continuous irradiation in cancer HeLa and normal Hs27 cells. Benzoxazole cyanine dyes are more photostable under direct irradiation than benzothiazole ones (Figure 6a). Increasing the length of the polymethine chain for cyanine was shown to reduce photostability.[52] After 1 min 30 s of

https://doi.org/10.1021/acsomega.2c05231
ACS Omega 2022, 7, 47734−47746

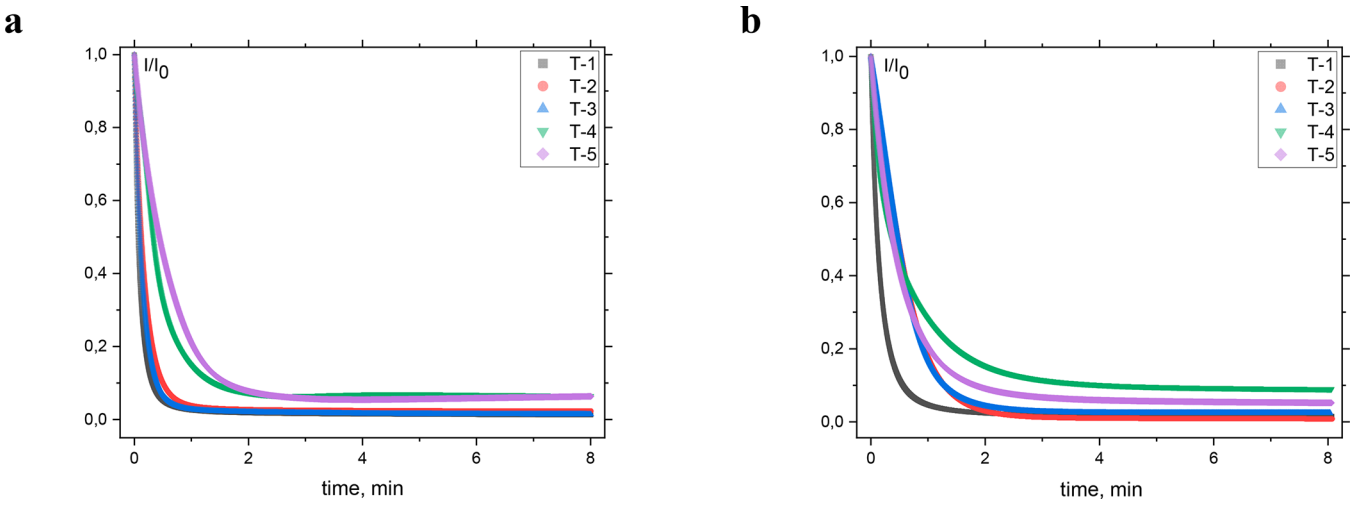

Figure 6. Time-dependent confocal fluorescence microscopy imaging of HeLa (a) and Hs27 (b) cells stained by trimethine cyanine dyes **T-1**−**T-5** (at the concentration of 10 μM for **T-1**, 1 μM for **T-2**, **T-3**, 0.1 μM for **T-4** and **T-5** for Hs27, and the same for HeLa, but the concentration for **T-3** is 0.1 μM) under constant irradiation for 8 min.

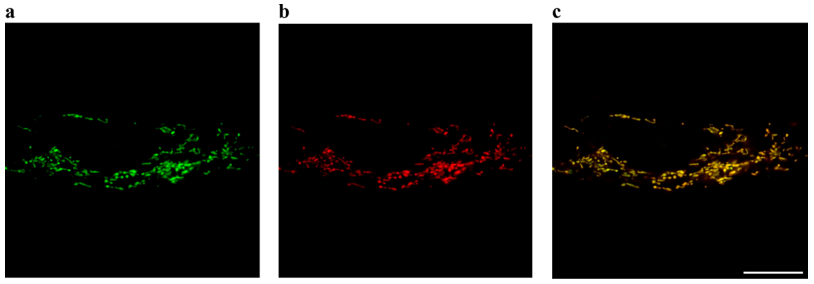

Figure 7. Fluorescence live-cell imaging of Hs27 cells. Colocalization analysis of the dye **T-5** (green, a) with MitoTracker CMXRos Red (red, b) and merged image (c). Scale bars: 10 μm.

constant irradiation in Hs27 cells, benzoxazole **T-4** and **T-5** remain at 22% and 15% of their fluorescence intensity, respectively. In the case of HeLa cells, they remain at 10% and 15% of fluorescence intensity.

In contrast, dyes **T-2**/**T-3** in Hs27 cells were up to 2 times less photostable (and the dye **T-1** is ∼7 times less stable compared to **T-4**). All benzothiazoles in HeLa cells are 7 times less stable than benzoxazoles. However, a lower concentration of **T-3** (0.1 μM) had to be used in cancer cells due to the signal's overbrightness. Similar results were previously shown on monomethine cyanine dyes, where benzoxazole derivative was ∼5 times more photostable than benzothiazoles.[19] We suggest that a heavy atom in the heterocycle of benzoxazole reduces the effective length of the π-electron system (thus, the length of the polymethine chain), positively affecting the stability of **T-4** and **T-5** dyes. The obtained photostability results are consistent with the location of the absorption maximums and the relation between the polymethine chain length and photostability. We assume symmetrical cationic benzoxazole cyanines as more suitable probes for cell visualization, and the dye **T-5** was chosen for further studies.

Cells Staining by the Benzoxazole Dye T-5 and Its Colocalization with MitoTracker CMXRos Red. **T-5** staining ability was examined in another cancer cell line—A2780. At a working concentration equal to 0.1 μM, the same staining pattern as above was shown: the dye could penetrate inside the cell, without penetration through the nuclear membrane and stain some structures inside the cytoplasm (Figure S4b). Also, as already shown for MCF-7, this dye lost its specificity to these structures in the higher concentration. At 1 μM, **T-5** brightly stains cytoplasm in A2780 cells entirely without any specificity and penetrates the nucleus staining nucleoli (Figure S4a). Colocalization of **T-5** and lysosome-targeting standard dye LysoTracker DeepRed (50 nM) was carried out to understand the specificity of the dye in cell imaging (Figure S5). This study showed no colocalization of **T-5** with LysoTracker DeepRed. Thus, the dye in a low concentration does not penetrate the nucleus and does not colocalize with lysosomes in the cytoplasm.

We have shown that the dye **T-5** is membrane-permeant and stains some compartments in cell cytoplasm at a concentration of 0.1 μM in all studied cell lines. It was assumed as a pattern of mitochondria staining. Thus, a colocalization analysis was carried out for the benzoxazole cyanine dye **T-5** with the MitoTracker CMXRos Red (a dye specific for mitochondria). As seen in Figure 7c, **T-5** shows signals overlapping with the mitochondria-targeting dye MitoTracker CMXRos Red with Person's value $r = 0.92 \pm 0.04$, proving its mitochondria localization (7 separate calculations are given in Figure S6).

CONCLUSIONS

We have presented the synthesis of cationic symmetrical trimethine cyanine dyes and discussed their spectral-luminescence properties and applicability in cell imaging. All dyes exhibit a strong fluorescent 'light-up' response in the presence of nucleic acids, including RNA and double-stranded DNA.

https://doi.org/10.1021/acsomega.2c05231
ACS Omega 2022, 7, 47734−47746

Wavelengths of fluorescence maxima of these dyes depend on heterocycles in dyes structures: benzoxazole trimethine cyanine fluorescence in a free state is observed on 501−506 nm, while dyes with benzothiazole heterocycle have a maximum of 564−580 nm with excitation wavelength nearly on 490 and 550−560 nm, respectively. These dyes possess low to moderate fluorescence intensity in the aqueous buffer. The addition of nucleic acids leads to an increase in fluorescence intensity (15−111 times). Spectral methods showed the binding of all dyes to nucleic acids, and different interaction mechanisms have been proposed.

The ability to visualize cell components of the studied dyes was tested on different cell lines (MCF-7, A2780, HeLa, Hs27). We have shown that all dyes are cell-permeant staining nucleus components, probably RNA-rich nucleoli with background fluorescence in the cytoplasm, except for the dye **T-5**, which at a concentration of 0.1 μM, specifically stains some structures in the cytoplasm. Colocalization analysis of the dye **T-5** with MitoTracker CMXRos Red shows that the **T-5** dye stains mitochondria (Pearson's Coefficient value = 0.92 ± 0.04). Fluorescence imaging of Hs27 cells by dye **T-5** shows no difference in mitochondrial selectivity between normal and cancer cells. The photostability study of dyes in cells under constant irradiation showed that benzoxazole dyes are up to ∼7 times more photostable than benzothiazole ones. Moreover, studied benzoxazoles are less cytotoxic to cancer cells at working concentrations than benzothiazoles (67% of cell viability compared to 12% for **T-1** and ∼30% for **T-2**, **T-3** after 24 h).

Because of its sensitive fluorescence response to nucleic acids with a significant fluorescence increase, moderate photostability, and low cytotoxicity, benzoxazole **T-4** dye can be used for nucleic acid detection *in vitro* and intracellular fluorescence imaging in live and fixed cells. On the other hand, the benzoxazole dye **T-5** is proposed as a good alternative to commercial dyes for mitochondria staining in the green-yellow region of the spectrum.

■ ASSOCIATED CONTENT

Supporting Information

The Supporting Information is available free of charge at https://pubs.acs.org/doi/10.1021/acsomega.2c05231.

> The absorption spectra of trimethine cyanines in MeOH, in 0.05 M Tris-HCl pH 7.9, in dsDNA presence and RNA presence; luminescent properties of trimethine cyanines in the presence of globular proteins; fluorescence live-cell imaging of A2780, HeLa cells, and colocalization experiment with LysoTracker DeepRed using A2780; separate merged CLSM images and Pearson's coefficient for colocalization of **T-5** with MitoTracker CMXRos Red using Hs27 (PDF)

■ AUTHOR INFORMATION

Corresponding Author

Svitlana Chernii − *Institute of Molecular Biology and Genetics NASU, 03143 Kyiv, Ukraine; V.I. Vernadsky Institute of General and Inorganic Chemistry NASU, 03142 Kyiv, Ukraine;* orcid.org/0000-0003-2034-8429; Email: chernii.sv@gmail.com

Authors

Daria Aristova − *Institute of Molecular Biology and Genetics NASU, 03143 Kyiv, Ukraine; Instituto Gulbenkian de Ciência, 2780-156 Oeiras, Portugal*

Roman Selin − *V.I. Vernadsky Institute of General and Inorganic Chemistry NASU, 03142 Kyiv, Ukraine; Organic Chemistry II, Friedrich-Alexander-University of Erlangen-Nuremberg, 91058 Erlangen, Germany*

Hannah Sophie Heil − *Instituto Gulbenkian de Ciência, 2780-156 Oeiras, Portugal*

Viktoriia Kosach − *Institute of Molecular Biology and Genetics NASU, 03143 Kyiv, Ukraine*

Yuriy Slominsky − *Institute of Organic Chemistry NASU, 02094 Kyiv, Ukraine*

Sergiy Yarmoluk − *Institute of Molecular Biology and Genetics NASU, 03143 Kyiv, Ukraine*

Vasyl Pekhnyo − *V.I. Vernadsky Institute of General and Inorganic Chemistry NASU, 03142 Kyiv, Ukraine*

[#]Vladyslava Kovalska − *Institute of Molecular Biology and Genetics NASU, 03143 Kyiv, Ukraine*

Ricardo Henriques − *Instituto Gulbenkian de Ciência, 2780-156 Oeiras, Portugal*

Andriy Mokhir − *Organic Chemistry II, Friedrich-Alexander-University of Erlangen-Nuremberg, 91058 Erlangen, Germany;* orcid.org/0000-0002-9079-5569

Complete contact information is available at: https://pubs.acs.org/10.1021/acsomega.2c05231

Author Contributions

Conceptualization: Vladyslava Kovalska. Formal analysis: Svitlana Chernii, Selin Roman, Daria Aristova, Hannah Sophie Heil. Investigation: Daria Aristova, Svitlana Chernii, Hannah Sophie Heil, Viktoriia Kosach, Roman Selin. Methodology: Yuriy Slominsky. Project administration: Andriy Mokhir, Ricardo Henriques. Resources: Andriy Mokhir, Ricardo Henriques, Vasyl Pekhnyo. Supervision: Andriy Mokhir, Ricardo Henriques. Validation: Vasyl Pekhnyo, Sergiy Yarmoluk. Visualization: Svitlana Chernii, Daria Aristova. Writing−original draft: Svitlana Chernii, Daria Aristova, Hannah Sophie Heil. Writing−review and editing: Andriy Mokhir, Ricardo Henriques, Svitlana Chernii, Daria Aristova. The authors have read and agreed to the published version of the manuscript.

Notes

The funders had no role in the design of the study; in the collection, analyses, or interpretation of data; in the writing of the manuscript; or in the decision to publish the results.

The authors declare no competing financial interest.

[#]Dr. Vladyslava Kovalska, who initiated and inspired this work, suddenly passed away on 03 December 2020.

■ ACKNOWLEDGMENTS

D.A., R.S., A.M., and S.Ch. are supported by the European Union's Horizon 2020 research and innovation programme under the Marie Skłodowska-Curie grant agreement No. 872331: "NoBiasFluors". In addition, S.Ch. and R.S. thank the grant of a group of young scientists of NAS of Ukraine No. 0122U002204 for 2022−2023. D.A., H.S.H, and R.H. also received support from the European Research Council (ERC) under the European Union's Horizon 2020 research and innovation programme (grant agreement No. 101001332), Horizon 2021 INFRA programme (grant agreement No. 101057970), the European Molecular Biology Organization

(EMBO) Installation Grant (EMBO-2020-IG4734), the Chan Zuckerberg Initiative Visual Proteomics Grant (vpi-0000000044). H.S.H. is supported by European Molecular Biology Organization (ALTF 499-2021) and Fundação para a Ciência e Tecnologia, Portugal (FCT) fellowship CEECIND/01480/2021.

REFERENCES

(1) Hickey, S. M.; Ung, B.; Bader, C.; Brooks, R.; Lazniewska, J.; Johnson, I. R. D.; Sorvina, A.; Logan, J.; Martini, C.; Moore, C. R.; Karageorgos, L.; Sweetman, M. J.; Brooks, D. A. Fluorescence Microscopy − An Outline of Hardware, Biological Handling, and Fluorophore Considerations. *Cells* **2022**, *11* (1), 35.

(2) Ettinger, A.; Wittmann, T. Fluorescence live cell imaging. *Methods Cell Biol.* **2014**, *123*, 77−94.

(3) Hua, X.-W.; Bao, Y.-W.; Zeng, J.; Wu, F.-G. Nucleolus-Targeted Red Emissive Carbon Dots with Polarity-Sensitive and Excitation-Independent Fluorescence Emission: High-Resolution Cell Imaging and in Vivo Tracking. *ACS Appl. Mater. Interfaces.* **2019**, *11* (36), 32647−32658.

(4) Hua, X.-W.; Bao, Y.-W.; Wu, F.-G. Fluorescent Carbon Quantum Dots with Intrinsic Nucleolus-Targeting Capability for Nucleolus Imaging and Enhanced Cytosolic and Nuclear Drug Delivery. *ACS Appl. Mater. Interfaces.* **2018**, *10* (13), 10664−10677.

(5) Liu, J.; Li, R.; Yang, B. Carbon Dots: A New Type of Carbon-Based Nanomaterial with Wide Applications. *ACS Cent. Sci.* **2020**, *6* (12), 2179−2195.

(6) Specht, E. A.; Braselmann, E.; Palmer, A. E. A Critical and Comparative Review of Fluorescent Tools for Live-Cell Imaging. *Annu. Rev. Physiol.* **2017**, *79*, 93−117.

(7) Williams, C. XXVI.—Researches on Chinoline and its Homologues. *Trans. - R. Soc. Edinburgh* **1857**, *21*, 377−401.

(8) Ma, X.; Shi, L.; Zhang, B.; Liu, L.; Fu, Y.; Zhang, X. Recent advances in bioprobes and biolabels based on cyanine dyes. *Anal. Bioanal. Chem.* **2022**, *414*, 4551−4573.

(9) Sun, W.; Guo, S.; Hu, Ch.; Fan, J.; Peng, X. Recent Development of Chemosensors Based on Cyanine Platforms. *Chem. Rev.* **2016**, *116*, 7768−7817.

(10) Yarmoluk, S.; Kovalska, V.; Volkova, K. Optimized dyes for protein and nucleic acid detection. *Springer Ser. Fluoresc* **2011**, *113*, 161−199.

(11) Jones, L. J.; Singer, V. L. Fluorescence Microplate-Based Assay for Tumor Necrosis Factor Activity Using SYTOX Green Stain. *Anal. Biochem.* **2001**, *293*, 8−15.

(12) Roth, B. L.; Poot, M.; Yue, S. T.; Millard, P. J. Bacterial viability and antibiotic susceptibility testing with SYTOX green nucleic acid stain. *Appl. Environ. Microbiol.* **1997**, *63*, 2421−31.

(13) Lebaron, P.; Catala, P.; Parthuisot, N. Effectiveness of SYTOX Green stain for bacterial viability assessment. *Appl. Environ. Microbiol.* **1998**, *64*, 2697−700.

(14) Johnson, I. D.; Spence, M. T. Z. *The Molecular Probes Handbook: A Guide To Fluorescent Probes And Labeling Technologies*, 11th ed.; Academic Press, Life Technologies: Carlsbad, CA, USA, 2010, 307−314.

(15) Pronkin, P. G.; Tatikolov, A. S. Photonics of Trimethine Cyanine Dyes as Probes for Biomolecules. *Molecules* **2022**, *27*, 6367.

(16) Moreira, B. G.; You, Y.; Owczarzy, R. Cy3 and Cy5 dyes attached to oligonucleotide terminus stabilize DNA duplexes: predictive thermodynamic model. *Biophys Chem.* **2015**, *198*, 36−44.

(17) Suzuki, T.; Fujikura, K.; Higashiyama, T.; Takata, K. DNA Staining for Fluorescence and Laser Confocal Microscopy. *J. Histochem. Cytochem.* **1997**, *45*, 49−53.

(18) Ohulchanskyy, T. Yu; Pudavar, H. E.; Yarmoluk, S. M.; Yashchuk, V. M.; Bergey, E. G.; Prasad, P. N. A monomethine cyanine dye Cyan 40 for two-photon-excited fluorescence detection of nucleic acids and their visualization in live cells. *Photochem. Photobiol.* **2003**, *77*, 138−145.

(19) Aristova, D.; Kosach, V.; Chernii, S.; Slominsky, Yu.; Balanda, A.; Filonenko, V.; Yarmoluk, S.; Rotaru, A.; Ozkan, H. G.; Mokhir, A.; Kovalska, V. Monomethine cyanine probes for visualization of cellular RNA by fluorescence microscopy. *Methods Appl. Fluoresc.* **2021**, *9*, 045002.

(20) Aristova, D.; Volynets, G.; Chernii, S.; Losytskyy, M.; Balanda, A.; Slominskii, Y.; Mokhir, A.; Yarmoluk, S.; Kovalska, V. Far-red pentamethine cyanine dyes as fluorescent probes for the detection of serum albumins. *R. Soc. Open Sci.* **2020**, *7*, 200453.

(21) Syniugina, A.; Chernii, S.; Losytskyy, M.; Syniugin, A.; Slominskii, Y.; Balanda, A.; Yarmoluk, S.; et al. The synthesis and study of novel merocyanine probes for protein detection and cells visualization. *Photochem. Photobiol.* **2021**, *7*, 100046.

(22) Yarmoluk, S. M.; Kovalska, V. B.; Volkova, K. D. Optimized Dyes for Protein and Nucleic Acid Detection. *Springer Ser. Fluoresc.* **2011**, *113*, 161−199.

(23) Lukashov, S. S.; Losytskyy, M. Yu.; Slominskii, Yu. L.; Yarmoluk, S. M. Interaction of cyanine dyes with nucleic acids. 7. Carbocyanine dyes, substituted in polymethine chain, as possible probes for fluorescent nucleic acid detection [in Ukrainian]. *Biopolym. Cell.* **2001**, *17* (2), 169−177.

(24) Armitage, B. A. Armitage Cyanine Dye−Nucleic Acid Interactions. *Top. Heterocycl. Chem.* **2008**, *14*, 11−29.

(25) Anikovsky, M. Y.; Tatikolov, A. S.; Kuzmin, V. A. Fluorescent Properties of Some Thia- and Oxacarbocyanine Dyes in the Presence of DNA. *High Energy Chem.* **2002**, *36*, 179−183.

(26) Kiprianov, A. I.; Sych, K. D. *Zapysky Instytutu Khimii Akademii Nauk URSR [In Russian]* **1946**, *8*, 105−125.

(27) Hamer, F. M. *The cyanine dyes and related compounds. The chemistry of heterocyclic compounds. XVIII*; Academic Press: New York, 1964; p 790.

(28) Brooker, L. G. S.; White, F. L. Studies in the Cyanine Dye Series. II. Carbocyanines with Substituents in the Three-Carbon Chain. *J. Am. Chem. Soc.* **1935**, *57* (12), 2480−2488.

(29) Lukashov, S. S.; Makovenko, I. E.; Losytskyy, M.Yu.; Slominskii, Yu.L.; Yarmoluk, S. M. Interaction of cyanine dyes with nucleic acids. Meso-methylsubstituted trimethincyanines, as possible probes for fluorescent nucleic acid detection. *Biopolym. Cell.* **2001**, *17* (5), 448−454.

(30) Kabatc, J.; Pączkowski, J. The photophysical and photochemical properties of the oxacarbocyanine and thiacarbocyanine dyes. *Dyes Pigm.* **2004**, *61* (1), 1−16.

(31) Schindelin, J.; Arganda-Carreras, I.; Frise, E.; Kaynig, V.; Longair, M.; Pietzsch, T.; Preibisch, S.; Rueden, C.; Saalfeld, S.; Schmid, B.; Tinevez, J.; White, D.; Hartenstein, V.; Eliceiri, K.; Tomancak, P.; Cardona, A. Fiji: an open-source platform for biological-image analysis. *Nat. Methods.* **2012**, *9*, 676−682.

(32) Bolte, S.; Cordelières, F. P. A guided tour into subcellular co-localization analysis in light microscopy. *J. Microsc.* **2006**, *224*, 213−232.

(33) Levitus, M.; Ranjit, S. Cyanine dyes in biophysical research: The photophysics of polymethine fluorescent dyes in biomolecular environments. *Q. Rev. Biophys.* **2011**, *44* (1), 123−151.

(34) Pronkin, P.; Tatikolov, A. Isomerization and Properties of Isomers of Carbocyanine Dyes. *Sci.* **2019**, *1* (1), 19.

(35) Ryu, N.; Okazaki, Y.; Pouget, E.; Takafuji, M.; Nagaoka, S.; Ihara, H.; Oda, R. Fluorescence emission originated from the H-aggregated cyanine dye with chiral gemini surfactant assemblies having a narrow absorption band and a remarkably large Stokes shift. *Chem. Commun.* **2017**, *53* (63), 8870−8873.

(36) Bricks, J. L.; Slominskii, Y. L.; Panas, I. D.; Demchenko, A. P. Fluorescent J-aggregates of cyanine dyes: basic research and applications review. *Methods Appl. Fluoresc.* **2018**, *6* (1), 012001.

(37) Lukashov, S. S.; Kachkovskyy, G. O.; Losytskyy, M. Y.; Yarmoluk, S. M. The interaction of cyanine dyes with nucleic acids. 22. Spectral-luminescent properties of monomethine pyrylium and pyridinium cyanines and their DNA complexes [In Ukrainian]. *Biopolym. Cell.* **2001**, *17* (3), 242−248.

https://doi.org/10.1021/acsomega.2c05231
ACS Omega 2022, 7, 47734−47746

(38) Rösch, U.; Yao, S.; Wortmann, R.; Würthner, F. Fluorescent H-Aggregates of Merocyanine Dyes. *Angew. Chem.* **2006**, *118* (42), 7184−7188.
(39) Zhytniakivska, O.; Zabrudska, A.; Tarabara, U.; Vus, K.; Trusova, V.; Gorbenko, G.; Kurutos, A.; Deligeorgiev, T. Competitive Binding of Novel Cyanine Dye AK3−5 and Europium Coordination Complexes to DNA. *East Eur. J. Phys.* **2019**, *3*, 63−70.
(40) Yarmoluk, S. M.; Kovalska, V. B.; Kovtun, Yu.P. Interaction of cyanine dyes with nucleic acids. 5. Towards model of "half intercalation" of monomethyne cyanine dyes into double-stranded nucleic acids. *Biopolym. Cell.* **1999**, *15*, 75−82.
(41) Yarmoluk, S. M.; Lukashov, S. S.; Ogul'chansky, T.Yu.; Losytskyy, M.Yu.; Kornyushyna, O. S. Interaction of cyanine dyes with nucleic acids. XXI. Arguments for half- intercalation model of interaction. *Biopolymers.* **2001**, *62*, 219−227.
(42) Sovenyhazy, K. M.; Bordelon, J. A.; Petty, J. T. Spectroscopic studies of the multiple binding modes of a trimethine-bridged cyanine dye with DNA. *Nucleic Acids Res.* **2003**, *31* (10), 2561−2569.
(43) Ishchenko, A. A. Structure and spectral-luminescent properties of polymethine dyes. *Russ. Chem. Rev.* **1991**, *60* (8), 865−884.
(44) Yarmoluk, S.; Kovalska, V.; Losytskyy, M. Symmetric cyanine dyes for detecting nucleic acids. *Biotechnol. Histochem.* **2008**, *83* (3−4), 131−145.
(45) Thomas, J. R.; Hergenrother, P. J. Targeting RNA with Small Molecules. *Chem. Rev.* **2008**, *108* (4), 1171−1224.
(46) Comşa, Ş.; Cîmpean, A. M.; Raica, M. The Story of MCF-7 Breast Cancer Cell Line: 40 years of Experience in Research. *Anticancer Res.* **2015**, *35* (6), 3147−3154.
(47) Yang, M.; Brackenbury, W. J. Membrane potential and cancer progression. *Front Physiol.* **2013**, *4*, 185.
(48) Gillies, R. J.; Raghunand, N.; Karczmar, G. S.; Bhujwalla, Z. M. MRI of the tumor microenvironment. *J. Magn. Reson. Imaging.* **2002**, *16*, 430−450.
(49) Webb, B. A.; Chimenti, M.; Jacobson, M. P.; Barber, D. L. Dysregulated pH: A perfect storm for cancer progression. *Nat. Rev. Cancer.* **2011**, *11*, 671−677.
(50) White, K. A.; Grillo-Hill, B. K.; Barber, D. L. Cancer cell behaviors mediated by dysregulated pH dynamics at a glance. *J. Cell Sci.* **2017**, *130*, 663−669.
(51) Bhat, T. A.; Kumar, S.; Chaudhary, A. K.; Yadav, N.; Chandra, D. Restoration of mitochondria function as a target for cancer therapy. *Drug Discovery Today.* **2015**, *20*, 635−643.
(52) Pham, W.; Lai, W. F.; Weissleder, R.; Tung, C. H. High efficiency synthesis of a bioconjugatable near-infrared fluorochrome. *Bioconjugate Chem.* **2003**, *14*, 1048−51.

https://doi.org/10.1021/acsomega.2c05231
ACS Omega 2022, 7, 47734−47746